MIT Open Access Articles

3D Eulerian modeling of thin rectangular gas-solid fluidized beds: Estimation of the specularity coefficient and its effects on bubbling dynamics and circulation times

Massachusetts Institute of Technology

3D Eulerian modeling of thin rectangular gas-solid fluidized beds: Estimation of the specularity coefficient and its effects on bubbling dynamics and circulation times

C. Altantzis*, R.B. Bates, A.F. Ghoniem

Massachusetts Institute of Technology, Department of Mechanical Engineering
77 Massachusetts Ave., Cambridge, MA 02139, United States

Abstract

This study aims at investigating the influence of the wall boundary conditions and specifically the specularity coefficient on the fluidization behavior of a thin rectangular fluidized bed by means of 3D numerical simulation employing an Eulerian description of the gas and the solid phases. Thin rectangular fluidized beds have been extensively used in the research literature since it is assumed that the flow behaves like a simpler two-dimensional flow and hence they offer validation data for $2D$ simulations. However, the effects of the front and the back walls are significant, influencing the sensitivity of the fluidization hydrodynamics to the third dimension whose consideration is thus necessary. In order to investigate the influence of the specularity coefficient, ϕ (a parameter controlling the momentum transfer from the particles to the wall), on the fluidization hydrodynamics, a parametric analysis is conducted and the response of the bubble dynamics, reflecting the gas motion, and the circulation fluxes, displaying the solids motion, are examined in detail. The computational results are compared with available experimental data in order to determine the values of ϕ that lead to the accurate description of the fluidization hydrodynamics via a two-fold validation strategy which involves the calculation of the circulation time and the solids concentration maps. It is observed that the appropriate value of the specularity coefficient depends rather strongly on the superficial gas velocity of the bed.

Keywords: Fluidized bed, two-fluid model, pseudo-2D fluidized bed, circulation time, specularity coefficient

1. Introduction

Fluidized beds, owing to their excellent mass and heat transfer characteristics, constitute the most widely employed paradigm of gas-solid flow with applications ranging from energy and chemicals production to pharmaceutical and agricultural processing. The importance of these devices across many industrial fields renders the optimization of their operation a worthy modeling challenge. Experimental investigations will always be the most reliable tool for examining the main characteristics of physical or chemical processes but their cost, especially for industrial-scale processes, is often prohibitive. The ever increasing progress of computing power and

*Corresponding Author
Email address: caltantz@mit.edu, altantzis@gmail.com, Telephone number: +1 (617)253-5365

the development of efficient numerical methods, has contributed to establishing Computational Fluid Dynamics (CFD) as an indispensable tool for understanding the fundamentals of gas-solid hydrodynamics, optimizing the operation of fluidized beds, and complementing the experiments by overcoming their limitations.

Depending on the level of detail employed for the description of the physical interactions in gas-solid flows, many modeling approaches have been developed over that last two decades [1]. The most detailed description is the Discrete Particle Method (DPM) or Direct Numerical Simulation (DNS), where the solid phase consists of individual particles interacting with each other and with the continuous phase without the need of any closure model. The computational cost of this type of simulations is extremely high and hence its use is limited to small domains with relatively small number of particles. Another method combining the Lagrangian framework for the motion of particles with the Eulerian description of the continuous phase is the Discrete Element Method (DEM). The computational cost of DEM is lower compared to the DNS since the closure of the inter-phase momentum exchange is modeled through a drag term resulting in lowering the demand for resolution. The most widely used approach for the simulation of gas-solid flows is the Two Fluid Model (TFM) which balances modeling fidelity and computational efficiency [2]. In TFM both the gas and the solid phases are considered as inter-penetrating continua and they are modeled in the Eulerian framework, thus reducing drastically the degrees of freedom compared to the DNS. The improvement in computational efficiency comes at the cost of the requirement of closure formulations for the modeling of the particle-particle and particle-gas interactions in the Eulerian model, rendering the modeling more complex and less accurate by increasing its dependency on tuning parameters.

In the framework of the Eulerian description of each phase, it is important to choose the proper boundary conditions for the velocities. For the vast majority of applications, a no-slip wall boundary condition is used for the gas phase, while a partial-slip condition is considered the most suitable for the solid phase. There exist several models for the solids slip velocity at the wall for the TFM [3–5], but owing to its simplicity and sound physical foundation, the model proposed by Johnson and Jackson [3] is the most widely used. This model, in order to define the slip velocity of the solids along the wall, considers the momentum transfer to the wall in the tangential direction both through the collisions of the particles characterized by the specularity coefficient, ϕ, and the sliding of the particles characterized by the Coulomb friction. The influence of the boundary conditions on the fluidization hydrodynamics is an area of active research enriched by the growing number of studies on the proper description of the wall boundary conditions. Unfortunately, due to the limitations of measurement techniques, the literature on experimental investigation of the particle wall collisions is very narrow. In [6], the authors investigated the influence of the wall roughness on the rebound of the particles in a horizontal channel flow using particle image velocimetry and extracting useful modeling parameters for Lagrangian particle simulations. Recently, Hernandez-Jimenez et al. [7] quantified experimentally the particle-wall frictional forces by processing the measured pressure signal with data of the solids motion extracted from

digital image analysis in a vertical thin rectangular bed. Both studies exemplify the significant influence of the wall boundary conditions on the solids motion but do not give information on the parameters involved in the Johnson-Jackson formulation.

The sensitivity of the fluidization hydrodynamics to the parameters of the boundary conditions is stressed in a continually growing number of computational studies (table 1). Benyahia et al. [8] conducted 2D axisymmetric simulations of dilute turbulent gas-solid flow in a cylinder and showed that values of ϕ close to 0 were preferred. Later, Almuttahar et al. [9] confirmed the predictions of [8] in 2D simulations of a circulating fluidized bed (CFB) by showing that using a free slip boundary condition, the near-wall solids volume fraction was in better agreement with experimental data. In their parametric study, they used only four values for ϕ, namely 0, 0.1, 0.5 and 1. Li et al. [10] performed 2D and 3D simulations investigating the gas mixing in cylindrical bubbling fluidized beds (BFB) and showed that gas back mixing is significantly influenced by the specularity coefficient. For the values of ϕ tested (table 1), more accurate description of the hydrodynamics was achieved for the lower values (0.0005). A more thorough study on a realistic 3D geometry of a thin rectangular bed was presented by Li et al. in [11]. The authors used a wide range of specularity coefficients (table 1) and compared the numerical predictions with experimental data for time averaged solids velocities profiles at different bed heights and evolution of bubble diameter with bed height. Although they did not conclude on a definitive value for the specularity coefficient, they exemplified its significant effect on bubble dynamics and showed that the 2D simulations are not sufficient for quantitative agreement with the experimental results - at least for the case of the thin rectangular beds. Zhong et al [12], analyzed the segregation and mixing of binary mixtures by means of 2D simulations and showed that for low values of ϕ (0, 0.0005), no segregation occurs, while the mixing is not influenced for a wide range of ϕ. Recent 2D computational studies of a spouted fluidized bed (SFB) [13] and of a bubbling bed concluded that free slip and low specularity coefficients resulted in deviations from the experimental data. A summary of the details of each of the studies mentioned above is shown in table 1. According to the validation studies, low values of the specularity coefficients are needed for high superficial gas velocity risers, while better agreement is attained with higher values of ϕ for bubbling beds indicating that the specularity coefficient is not a constant depending only on the wall roughness and the particle characteristics but also on the particle slip velocity. Li and Benyahia [14] derived a formulation for the specularity coefficient that takes into account the dependency on the flow characteristics and later [15] they implemented their model and conducted 2D simulations of a bubbling bed in order to calculate the correct values of ϕ.

The validation procedure, common in most of the above mentioned studies, involves the comparison of computed and experimentally measured quantities like the bed heights, the time averaged voidages and solids velocities profiles at different bed heights and the variation of bubble diameters across the bed. Although the quantities chosen are useful, offer a basis for validation and are indicative of the fluidization behavior, they do not lead to conclusive answers. As such, in most of the studies, while the authors stress the significance

of the specularity coefficient, they do not identify a correct value for ϕ but rather define a range of possibly correct values. In the current study, attention is focused on other quantities, namely the circulation flux and the circulation time, which combines information for solids motion and for bubble dynamics. By investigating the sensitivity of this quantity to the specularity coefficient, novel conclusions regarding the appropriate choice of specularity coefficient are identified. The circulation flux is defined as the mass flow of the solids moving either upwards or downwards averaged over the respective cross-sectional areas [16]. Attempts to measure the solids turnover rate in a fluidized bed began more than 60 years ago by Leva and Grummer [17]. Early experimental attempts to measure the solids circulation flux were based on the analysis of the motion of solids tracers [18].

In lieu of direct experimental data, it has also been common to apply the two-phase theory to correlate the shape and size of bubbles to the axial motion of solids [19]. Three of the most commonly used correlations are summarized in table 2. They depend on the superficial gas velocity U_{in}, the minimum fluidization velocity U_{mf}, the particle diameter d_m, the volume fraction of the gas phase at minimum fluidization, $\varepsilon_{g,mf}$ and the particle density ρ_m. The correlation proposed in [16] depends also on three adjustable parameters (Y, β_w, β_d) related to the conditions of the system. A linear dependence of solids circulation flux on the excess gas velocity defined as $(U_{in} - U_{mf})$ is due to the increase in flow through the bubble phase. Stein et al. [20] and later Fan et al. [21] used radioactive tracer particles combined with positron emission particle tracking (PEPT) to measure solids circulation frequency (inverse of solid circulation times) in a cylindrical bed. The former corroborated the near linear dependence of circulation frequency on the excess gas velocity common to all the correlations in table 2 and showed that the upward particle velocities were roughly 0.5 of the predicted bubble rise velocities. In a study of solids circulation in a thin rectangular bed (pseudo-2D) using particle image velocimetry and digital image analysis (PIV/DIA), the upward particle velocities were found to be only 0.2 of predicted bubble rise velocities [22]. To date there has been only one study which simultaneously measured the upward solids velocity of particles and bubble velocity. This work, done by Ohki and Shirai [23], found that upward velocity of solids was 0.35 of the upward bubble velocities. Nevertheless, while these correlations are potentially useful for order of magnitude estimation of the circulation time in large diameter 3D cylindrical beds, they have dubious applicability in the case of cylindrical beds with small diameters or rectangular beds with small thickness where wall effects are important.

The current study aims at investigating the influence of the specularity coefficient on the fluidization behavior of a thin rectangular bed by means of 3D numerical simulation. The front and back walls, being so close in a thin bed, influence the solids motion and the 2D assumption is strongly inaccurate as will be discussed in sec.5.1. The sensitivity of the solids circulation flux to variations of ϕ is studied together with detailed analysis of the differences in bubbling dynamics. Finally the appropriate values of ϕ for different conditions extracted from the simulations are validated with the experimental results presented in [24]. The validation procedure is a two-fold strategy since we compare circulation times, derived from the circulation fluxes, as well as solid

4

concentration maps, indicative of the time-averaged bubble presence across the bed.

2. Hydrodynamic model and simulation setup

2.1. Governing equations

In the current work, an Eulerian multiphase approach, where both gas and solid phases are described as interpenetrating continua, is employed for modelling the fluidization hydrodynamics, hence the solid phase is governed by Navier-Stokes type equations with the appropriate closure terms describing the gas-solid interactions and the particle-particle collisions. The conservation equations for mass and momentum are solved for the gas and for each of the solid phases:

Gas phase continuity

$$\frac{\partial}{\partial t}\left(\varepsilon_g \rho_g\right) + \nabla \cdot \left(\varepsilon_g \rho_g \vec{u}_g\right) = 0 \tag{1}$$

Solid phase continuity

$$\frac{\partial}{\partial t}\left(\varepsilon_m \rho_m\right) + \nabla \cdot \left(\varepsilon_m \rho_m \vec{u}_m\right) = 0 \tag{2}$$

Gas phase momentum

$$\frac{\partial}{\partial t}\left(\varepsilon_g \rho_g \vec{u}_g\right) + \nabla \cdot \left(\varepsilon_g \rho_g \vec{u}_g \vec{u}_g\right) = \nabla \cdot \bar{\bar{\tau}}_g - \varepsilon_g \nabla P_g + \varepsilon_g \rho_g \vec{g} - \vec{I}_{gm} \tag{3}$$

Solid phase momentum

$$\frac{\partial}{\partial t}\left(\varepsilon_m \rho_m \vec{u}_m\right) + \nabla \cdot \left(\varepsilon_m \rho_m \vec{u}_m \vec{u}_m\right) = \nabla \cdot \bar{\bar{S}}_m - \varepsilon_m \nabla P_g + \varepsilon_m \rho_m \vec{g} + \vec{I}_{gm} \tag{4}$$

Where ε, ρ and u are the volume fraction, the density and the velocity of each phase and the subscripts g and m indicate the gas and the solid phases respectively. P_g is the gas pressure, $\vec{g}$ is the gravitational acceleration, $\varepsilon_m \nabla P_g$ is the buoyancy effect on the solid phase and $\vec{I}_{gm}$ is the interphase momentum exchange term involving the drag force. Finally $\bar{\bar{\tau}}_g$ and $\bar{\bar{S}}_m$ are the gas and the solids stress tensors respectively.

A typical Newtonian closure is employed for the description of the gas stress tensor, while the closure expression for the solids stress tensor is based on the local solids volume fraction defining the granular flow regime. When the local solids volume fraction is lower than a critical value (viscous regime), the stresses arise from the collisions between the particles and their translation in the flow field. On the other hand, when the solids are densely packed and their volume fraction is high, the translational motion of the particles is hindered (plastic regime) and the theory of Schaeffer [25] is employed to model the pronounced effects of friction. The critical voidage below which friction is the main component of the solids stress tensor is determined by the maximum packing limit of the solids. The general form of the stress tensors are:

5

Gas phase stress tensor

$$\bar{\bar{\tau}}_g = \varepsilon_g \mu_g \left[\nabla \vec{u}_g + (\nabla \vec{u}_g)^T \right] - \frac{2}{3} \varepsilon_g \mu_g \nabla \cdot \vec{u}_g \bar{\bar{I}} \tag{5}$$

Solid phase stress tensor

$$\bar{\bar{S}}_m = \begin{cases} -P_m^p \bar{\bar{I}} + \bar{\bar{\tau}}_m^p, & \text{if } \varepsilon_g \leq \varepsilon_g^* \\ -P_m^v \bar{\bar{I}} + \bar{\bar{\tau}}_m^v, & \text{if } \varepsilon_g > \varepsilon_g^* \end{cases} \tag{6}$$

with μ_g being the gas viscosity and P_m and $\bar{\bar{\tau}}_m$ the pressure and the viscous stress of the solid phase. The superscripts p and v refer to the plastic and the viscous regime of the granular flow respectively, while $\bar{\bar{I}}$ is the unity tensor.

The Kinetic Theory of Granular Flows (KTGF) is used for the evaluation of the solid phase pressure and viscosity. KTGF considers the nature of the particle motion to be analogous to the motion of gas molecules, thus assuming that the random particle velocity follows a Maxwellian distribution. Granular temperature $|Theta$, is then introduced in order to model the energy of the random motion of the particles ([26, 27]). A transport equation is solved for this quantity:

Granular temperature

$$\frac{3}{2} \left[\frac{\partial (\varepsilon_m \rho_m \Theta_m)}{\partial t} + \nabla \cdot (\varepsilon_m \rho_m \vec{u}_m \Theta_m) \right] = \bar{\bar{S}}_m : \nabla \vec{u}_m + \nabla \cdot \vec{q}_{\Theta_m} - \gamma_{\Theta_m} + J_{vis} \tag{7}$$

with the right hand side consisting of a production term ($\bar{\bar{S}}_m : \nabla \vec{u}_m$), a diffusion term ($\nabla \cdot \vec{q}_{\Theta_m}$) and two dissipation terms accounting for the energy losses due to inelastic collisions (γ_{Θ_m}) and fluid viscosity (J_{vis}).

The drag law describing the interphase momentum exchange between the gas and solids phases is derived by Gidaspow [27] and is a combination of the Ergun model for dense regimes and the Wen and Yu equation for dilute regimes. The buoyancy effects are already incorporated in the pressure gradient terms in the right hand sides of the momentum equations for each of the phases in the mixture.

Gas-solids drag law

$$\vec{I}_{gm} = \beta \left(\vec{u}_g - \vec{u}_m \right) \tag{8}$$

$$\beta = \begin{cases} 150 \frac{\varepsilon_m^2 \mu_g}{\varepsilon_g d_m^2} + 1.75 \frac{\varepsilon_m \rho_g |\vec{u}_m - \vec{u}_g|}{d_m}, & \text{if } \varepsilon_g \leq 0.8 \\ \frac{3}{4} C_d \varepsilon_g^{-2.65} \frac{\varepsilon_m \varepsilon_g \rho_g |\vec{u}_m - \vec{u}_g|}{d_m}, & \text{if } \varepsilon_g > 0.8 \end{cases}$$

$$C_d = \begin{cases} \frac{24}{Re_m} \left(1_0.15 Re_m^{0.687} \right), & \text{if } Re_m < 1000 \\ 0.44, & \text{if } Re_m \geq 1000 \end{cases}$$

$$Re_m = \frac{\rho_g \varepsilon_g d_m |\vec{u}_m - \vec{u}_g|}{\mu_g}$$

The numerical tool used to solve the governing equations is the Multiphase Flow with Interphase eXchanges (MFIX) code developed by the U.S. Department of Energy (DOE) National Energy Technology Laboratory (NETL). MFIX is a general-purpose open-source code for the simulation of gas-solid system hydrodynamics accounting also for heat transfer and chemical reactions (https://mfix.netl.doe.gov). Documentation on the theoretical expressions implemented in the code, as well as further details about the constitutive relations for each of the temrs appearing in the equations discussed above, can be found in [28].

2.2. Simulation setup

The simulation setup is based on the experimental work of Sanchez-Delgado et al. [24]. The authors employed a combination of two non-intrusive techniques, namely Particle Image Velocimetry (PIV) and Digital Image Analysis (DIA) on a thin rectangular bed with a cross-section of 0.5×50 cm and a height of 150 cm. The front side of the bed was transparent so that visual observations are possible. The fluidizing medium was air and the solid phase consisted of spherical glass particles with $\rho_m = 2500$ kg/m^3 and diameters between 600 μm to 800 μm. The particle size distribution is normal with the mean being 677.8 μm and the standard deviation equal to 93.3 μm. The DIA is used in order to distinguish between the dense and the gas phases and the PIV determines the solids velocities. The combined information from the two techniques results in the extraction of the circulation time (average time needed for a particle to move from the bottom of the bed to the top and back to the bottom). Five different superficial gas velocities (U_{in}) and four static bed heights (h_{init}) were tested, resulting in a test matrix of twenty different cases. In addition, the authors provide time averaged solids concentration maps for a subset of the test matrix. To the best of our knowledge, this is the only study that provides circulation times in bubbling fluidized beds by means of PIV and DIA, and further details on the experimental setup are offered in [24, 29].

In this paper, a column of identical geometry to the experimental work is simulated in $3D$. The lateral (x) and vertical (y) directions are discretized with uniform cells with $\Delta x = \Delta y = 5$ mm, while 3 uniform cells are used along the z direction with $\Delta z = 5/3$ mm. In total, the computational domain is discretized with 90000

cells. The largest sides of the computational cells are approximately 7 times the particle size, ensuring that the resolution is high enough for the accurate descritization of the solid phase. At the same time, this level of resolution satisfies the optimal grid size criterion, discussed in [30], according to which the computational cells should be larger than the particle diameter.

The bed depth is intentionally chosen to be thin ($z = 0.5$ cm) in order to match the geometry of the experiment, resulting in a high surface to volume ratio of the fluidization space which in turn leads to a more pronounced interaction between the flow of both phases with the front and back walls. Thus, consideration of the full $3D$ problem, allows us to examine the influence of the boundary conditions on the fluidization hydrodynamics. From the twenty cases investigated in [24], we consider seven. Five cases with initial bed height of 30 cm and varying superficial gas velocities ($U_{in} = 2.5, 2.25, 2.0, 1.75$ and $1.5U_{mf}$) corresponding to cases A-E in [24] and two more cases with $h_{init} = 50$ cm and $U_{in} = 2.5U_{mf}$ and $U_{in} = 1.75U_{mf}$ (Cases K and N in [24]). It is specified in [24] that the minimum fluidization velocity depends on the initial bed height, so for the cases with $h_{init} = 30$ cm the minimum fluidization velocity is $U_{mf} = 43.17$ cm/s and for $h_{init} = 50$ cm, $U_{mf} = 49.3$ cm/s. The different cases considered in this study are presented in table 3, while details about the parameters of the numerical simulations, common to all the cases considered, are summarized in table 4.

The finite volume method is employed for the spatial discretization of the governing equations on a staggered grid. The velocity components are calculated at the centres of the cell faces, while the scalars are computed at the centres of the cells. The diffusion terms are discretized using a central differencing scheme and the superbee flux-limiter is employed for the convection terms. Both techniques ensure second order accuracy [31]. The numerical technique is based on the SIMPLE (Semi-Implicit Method for Pressure Linked Equations) algorithm [32]. Time integration is accomplished by a first order accurate forward Euler method employing a variable time step which is automatically adjusted to reduce the run time. A detailed description of the numerical implementation is presented in [31].

Uniform inflow gas velocity is specified at the bottom, while a constant pressure outflow is used at the top boundary of the domain. Along the walls, a no-slip boundary condition is used for the gas phase and a partial-slip boundary condition is adopted for the solids phases based on the formulation of Johnson and Jackson. In [3], the authors derive boundary conditions for the slip velocity ($\vec{u}_{sl}$) and the granular temperature of the solid phase on the wall:

$$\vec{n} \cdot \mu_m \nabla \vec{u}_{sl} = -\frac{\pi \phi \varepsilon_m \rho_m \vec{u}_{sl} g_0 \sqrt{3\Theta}}{6\varepsilon_{m,max}} \tag{9}$$

and

$$\vec{n} \cdot \kappa_m \nabla \Theta = -\frac{\pi \rho_m \varepsilon_m g_0 \vec{u}_{sl}^2}{6\varepsilon_{m,max}} - \frac{\pi \varepsilon_m \rho_m g_0 \Theta^{\frac{3}{2}} \sqrt{3}(1 - e_w^2)}{4\varepsilon_{m,max}} \tag{10}$$

where $\vec{n}$ is the unit vector normal to the wall, $\varepsilon_{m,max}$ is the maximum solids volume fraction, κ_m the

diffusion coefficient of the granular energy and g_0 is the radial distribution function which can interpreted as the average non-dimensional distance between spherical particles. The expression for g_0 is:

$$g_0 = \left[1 - \left(\frac{\varepsilon_m}{\varepsilon_{m,max}} \right)^{\frac{1}{3}} \right]^{-1} \tag{11}$$

The parameters characterizing the influence of the wall on the solids hydrodynamics are the wall-particle restitution coefficient e_w and the specularity coefficient ϕ. The former is a measure of the particle kinetic energy dissipated during the collisions. Sufficiently low values of e_w result in high granular energy dissipation and increased solids concentration in the near wall region [33]. For the typical values tested in the literature ($0.7 < e_w < 1$), it has been consistently shown that the value of e_w does not influence significantly the fluidization hydrodynamics [9, 11]. The specularity coefficient is a measure of the portion of the particle momentum transferred to the wall in the tangential direction during collisions, ranging from 0 for perfectly specular collisions and 1 for perfectly diffuse collisions. It has been shown that ϕ influences heavily the fluidization hydrodynamics and its accurate estimation is an area of active research. Its value depends on the wall roughness and it is difficult to be measured experimentally. The two-fold objective of this study is a systematic investigation of the influence of ϕ on the bed hydrodynamics as well as determining the values of ϕ which best represent the hydrodynamics of the experiment under consideration.

3. Bubble dynamics

As already mentioned in sec. 1, one of the objectives of the current study is the investigation of the impact of the specularity coefficient on the bubbling dynamics in a fluidized bed. The bubble analysis consists of two steps. In the first step we apply digital image analysis (DIA) to determine geometric statistics of the bubbles. The second step applies a lagrangian velocimetry technique (LVT) to extract information on the bubble velocities.

The DIA step was performed on the $3D$ rectangular multifluid Eulerian simulations using an algorithm similar to that employed in [11]. First, a series of $2D$ cross section images were generated from the simulation data at a time step of 0.02 seconds using ParaView software. Then, these images were converted to binary greyscale images using ImageJ software (http://rsbweb.nih.gov/ij/). A voidage threshold of $\varepsilon_g^* = 0.8$ was used to demarcate the boundaries between the bubble and emulsion phases. Bubbles in contact with boundaries (e.g open to the freeboard or touch the bed walls) were excluded from the analysis. The cross sectional area (A_b) and position of bubbles are identified in each image enabling the equivalent bubble diameter to be calculated, $d_b = \sqrt{4A_b/\pi}$. The averaging procedure used to calculate the mean bubble diameter, $\bar{d}_b$ at a particular height, is based on the arithmetic mean of the equivalent bubble diameters. A minimum equivalent bubble size threshold of $d_{b,min} = 0.01$ m was used. Since boundary-contacting bubbles were excluded, no maximum

bubble size threshold was set. From the digital image analysis (DIA) alone it is possible to obtain both local and spatio-temporal averaged statistics on the bubbles.

The bubble velocities were extracted using an LVT similar to that described first in [34]. The procedure works by comparing the displacement of bubbles between adjacent frames and applies filters so that only bubbles which translate at physically expected velocities are considered in the averaging process. The algorithm consists of the following steps:

I) N bubbles in the first frame and M bubbles second frame are numbered according to their height (distance from distributor) in the image. N and M are not necessarily equal but can be.

II) The velocity for bubble i $(i = 1, 2, ..N)$ in frame p, $(\vec{u}_{p,i})$ is computed by subtracting the distance between its x, y coordinate and that of the respective bubble j (where $j = i$) in the subsequent frame $(p + 1)$, and dividing by the time increment,

$$\vec{u}_{p,i} = \left(\frac{x_{p+1,j} - x_{p,i}}{\Delta t}, \frac{y_{p+1,j} - y_{p,i}}{\Delta t} \right) \tag{12}$$

III) Outliers are removed by filtering bubbles with the following conditions:

$$0 < u_{y_{p,i}} < u_{y_{max}}$$

$$|u_{x_{p,i}}| < u_{x_{max}}$$

The first condition limits the consideration to bubble moving with a positive upward velocity less than the maximum expected rise velocity $(u_{y_{max}})$. The second condition limits the absolute lateral velocity to be less than the maximum expected lateral velocity $(u_{x_{max}})$. The maximum expected rise velocity and the maximum expected lateral velocity are hard-coded parameters into the algorithm preventing the possible calculation of very large bubble velocities through erroneous linking of bubbles at consecutive time steps.

IV) Repeat steps I)-III) for all frames.

LVT enables the computation of the lateral and axial velocities for all bubbles. By combining the DIA (geometric statistics) with LVT the following can be obtained:

α) Average lateral and rise velocities as a function of height and diameter

β) Distributions of bubble rise angle

4. Circulation time

The validation strategy of this study involves the estimation of the solids circulation time and the identification of the parameters that result in agreement between the computational and the experimental results. The circulation time or bed turnover time is defined as the time needed for the solids to move from the bottom of the bed to the top and back to the bottom. Although this quantity constitutes a critical measure of the solids motion and mixing in a fluidized bed, it has not been widely considered in the literature mainly due to the

difficulty in measuring it experimentally. One of the few attempts to extract circulation time experimentally was presented in the recent study of Sanchez-Delgado et al. [24] as discussed in sec. 1. In the current section we present the procedure of extracting the circulation time from the simulations and discuss the differences between our procedure and how it is obtained from the experiments, elucidating the validation strategy discussed later in this work.

The solids flux $J_c(y)$ along the bed height (y-direction) is defined as

$$J(y) = \left\langle \frac{1}{A} \int\limits_{x_{min}}^{x_{max}} \int\limits_{z_{min}}^{z_{max}} (\rho_m \varepsilon_m v_m)\, dz dx \right\rangle \tag{13}$$

where A is the bed cross-sectional area, v_m is the vertical component of the solids velocity and the angle brackets indicate the time averaging operation of the normalized surface integral over each cross-section of the rectangular bed; the units of this quantity are $[kg/m^2 s]$. While the bed operates in a statistically steady state, at every cross-section, the solids move both upwards and downwards simultaneously in order for the total time averaged mass flow rate to remain constant. As a result, the proper definition of the circulation flux should take into account the direction of the motion of the solids, hence the upwards (positive) and the downwards (negative) circulation fluxes need to be identified. In order to calculate the fluxes while accounting for the part of the cross-section surface area where the motion of the solids is either positive or negative, instead of normalizing over the whole cross-section area of the bed, the direction-specific solid fluxes are defined by first identifying the area of each cross-section where the solids move either upwards (A^+) or downwards (A^-) at every time step, and then by calculating the time average of the surface integral of the local fluxes normalized over the respective areas

$$J_c^{+/-}(y) = \left\langle \frac{1}{A^{+/-}} \int\limits_{x_{min}^{+/-}}^{x_{max}^{+/-}} \int\limits_{z_{min}^{+/-}}^{z_{max}^{+/-}} \left(\rho_m \varepsilon_m^{+/-} v_m^{+/-} \right) dz dx \right\rangle \tag{14}$$

where the superscript of the quantities is used to distinguish between the upwards (positive) and the downwards (negative) moving solids.

The circulation time at every time instant and every point of the fluidized bed is calculated as the ratio of the amount of solids mass $m(x,y,z,t)$ moving either upwards or downwards over the corresponding mass flow rate $\dot{m}(x,y,z,t)$. Since we already distinguished between the positive and the negative solids motion, we define the respective circulation times accordingly.

$$\Delta t_c(x,y,z,t) = \frac{m(x,y,z,t)}{\dot{m}(x,y,z,t)} = \frac{\rho_m(x,y,z,t)\varepsilon_m(x,y,z,t)\Delta x \Delta y \Delta z}{\rho_m(x,y,z,t)\varepsilon_m(x,y,z,t)v_m(x,y,z,t)\Delta x \Delta z} = \frac{\Delta y}{v_m(x,y,z,t)} \tag{15}$$

The circulation times (t_c^+ and t_c^-) are calculated along the discretized y-direction for every y. The incremental

upwards or downwards circulation time is:

$$\Delta t_c^{+/-}(y) = \left\langle \frac{1}{A^{+/-}} \int\limits_{x_{min}^{+/-}}^{x_{max}^{+/-}} \int\limits_{z_{min}^{+/-}}^{z_{max}^{+/-}} \frac{\Delta y}{v_m^{+/-}(x,y,z,t)} dzdx \right\rangle \tag{16}$$

The upwards, t_c^+, and downwards, t_c^-, circulation times are obtained by integrating the incremental times over the bed height and the total circulation time, t_c, is the sum of the direction specific times

$$t_c = \int\limits_{y_{min}}^{y_{max}} \Delta t_c^+(y)dy + \int\limits_{y_{min}}^{y_{max}} \Delta t_c^-(y)dy \tag{17}$$

The combination of PIV and DIA, employed in [24], results in the measurement of the solids velocity in each of the investigation windows and the distinction between gas and emulsion phase on each window and the methodology for the extraction of the circulation time follows similar steps. First the time average upwards and downwards solids velocities profiles along the y-direction are extracted and then, after showing that these profiles are similar quantitatively, the circulation time is defined as

$$t_c = \int\limits_{y_{min}}^{y_{max}} \frac{2}{v_m^-(y)} dy \tag{18}$$

with

$$v_m^-(y) = \left| \frac{\int_{x_{min}}^{x_{max}} v_m^-(x,y)dx}{N} \right| \tag{19}$$

where N is the total number of investigation windows at different bed heights. Since the measurements are done in the thin rectangular bed in order to neglect the effect of the depth of the bed, the spatial averaging of the local solids velocities is considered only along the $x-$direction (lateral direction). The main difference lies in the spatial averaging over each cross-section. In [24], the authors, when defining either the upwards or the downwards solids velocity, normalize over the whole cross-sectional area instead of using only the part of the surface area where the solids either move upwards or downwards respectively. As a result, the measured solids velocity profiles along the bed are lower than the ones calculated by the methodology presented above. Furthermore, it is reported in [24] that the solids volume fraction in the dense phase is everywhere constant and hence, since the profiles of time averaged positive and negative mass flow rates along the $y-$direction should be equal, the upwards and downwards solids velocities are also equal. The assumption of a constant solids volume fraction everywhere in the emulsion phase is reasonably valid in the regions away from the bubbles. On the other hand, the spatial averaging of the solids velocities based on the normalization over the whole extent of the bed cross-section and not over the parts corresponding to either positive or negative solids motion results in obtaining higher circulation times. In the current study we apply the definition described above for the parametric analysis of the influence of the specularity coefficient on the circulation fluxes and times. On the other hand, for validating the computational results with the circulation times reported in the experiments we

employ the averaging methodology presented in [24].

5. Results and Discussion

5.1. Influence of specularity coefficient on bubble dynamics

To investigate the influence of the boundary conditions on the fluidization hydrodynamics, a thorough parametric study is conducted with respect to the specularity coefficient for two identical beds with different superficial gas velocities. The values of ϕ tested were $\phi = 0.0001, 0.0005, 0.001, 0.005, 0.001, 0.01, 0.05, 0.1$ and 0.5, while $U_{in} = 2.5U_{mf}$ and $1.75U_{mf}$. Figure 1 shows the solids holdup profiles for the two superficial gas velocity cases. For each case, only four out of the eight values of ϕ are plotted for clarity. In both cases, lower specularity coefficients resulted in higher solids holdup profiles with a more gradual decrease of the solids volume fraction indicating that the splashing zone is not only higher, but it is also more extended. For the case with $U_{in} = 2.5U_{mf}$, the extent of the splashing zones are approximately $0.3 < Y < 0.6$ and $0.4 < Y < 0.45$ for $\phi = 0.0005$ and $\phi = 0.5$ respectively, while the corresponding values for $U_{in} = 1.75U_{mf}$ are roughly $0.35 < Y < 0.5$ and $0.36 < Y < 0.4$. This difference suggests that the fluidization behavior tends toward the slugging regime for smaller ϕ. Also, the effect of the specularity coefficient is more pronounced for the high superficial gas velocity case since beds with high U_{in} are closer to the transition of the fluidization behavior.

The fluidization behavior is illustrated in figure 2(a-d), which shows instantaneous voidage contours in greyscale for the four specularity coefficients discussed in the previous plot for the case with $U_{in} = 2.5U_{mf}$. For $\phi = 0.0005$ (fig. 2(a)), the bubbles formed at the bottom of the bed are large and they merge very close to the inflow to create large slugs with diameter approximately equal with the bed width. The solids are pushed upwards as the slugs move and erupt at the center of the bed and then move downwards along the side walls under the influence of gravity. A similar picture of fluidization is shown in fig. 2(b) for $\phi = 0.005$. The fluidization behavior lies in the slugging regime but the size of the slugs is smaller than in the previous case. A completely different behavior is shown in fig. 2(c) for $\phi = 0.05$. A large number of small bubbles is formed at the bottom of the bed and while they ascent, they coalesce to form bubbles whose diameter is smaller than the bed width. It is also observed that the bubbles reaching the splashing zone do not erupt only at the center of the bed, since the initial bed height is not large enough, allowing for solids to move downwards at parts of the bed that are away from the side walls. Finally, the bubbling behavior for $\phi = 0.5$ is shown in fig. 2(d). Multiple eruption points are observed at the splashing zone, whose position does not change in time. Instead of proper fluidization, the hydrodynamic pattern is dominated by channeling effects and the bypassing of the gas almost straight towards the splashing zone without interacting sufficiently with the solid phase. Similar transitions are presented in fig. 3, which similar to fig. 2 but for the case with $U_{in} = 1.75U_{mf}$. It is observed that lower superficial gas velocity results in the appearance of a larger number of bubbles with smaller diameters. As the specularity coefficient decreases, the fluidization behavior tends towards the slugging regime for this case as

well, with the difference that the size of the formed slugs is smaller than the slugs formed in the high superficial gas velocity case.

The bubble size statistics extracted from the instantaneous images of the voidage contours are used for the description of the bubbling behavior. The results are shown in fig. 4 for $U_{in} = 2.5U_{mf}$. The sampling time was $3 < t < 30$ s, in order to avoid the startup effects, at a frequency of 100 Hz. Fig. 4(a) and (b) show the cumulative normalized frequency and the normalized frequency respectively of the bubble diameters for the four values of the specularity coefficients discussed above. The results generalize the description of the instantaneous images and confirm the observations discussed previously. Low specularity coefficients lead to the formation of larger bubbles and slugs; for example, for $\phi = 0.0005$, 20% of the bubbles have a diameter larger 10 cm, while the percentage for $\phi = 0.5$ is only 1%. For the latter case, 80% of the bubble diameters are below 5 cm. Fig. 4(b) shows that the frequency of the appearance of small bubbles ($d_b < 5$ cm) increases with increasing ϕ until $d_b = 6$ cm, where it is roughly equal for all the cases tested. Larger bubbles appear less frequently when $\phi > 0.005$. There are no bubbles with $d_b > 13$ cm for $\phi = 0.5$ and no bubbles with $d_b > 18$ cm for $\phi = 0.05$.

The bubble number density per frame is presented in fig. 5 for the two superficial gas velocities and the different values of ϕ tested. It should be noted that the specularity coefficient is represented on a logarithmic scale. For all values of ϕ the number density of bubbles per frame is higher for the low superficial gas velocity bed indicating the formation of small bubbles which coalesce further upwards. On the other hand, in the high superficial velocity bed, the bubbles are larger and in addition they coalesce at lower bed heights to form larger ones. The low superficial gas velocity bed operates in the bubbling regime for a wider range of specularity coefficients and tends towards the slugging behavior only for the lowest values of ϕ. The trend of the variation of the bubble number density per frame with ϕ does not depend on the superficial gas velocity. For high ϕ, the bed consists of a large number of bubbles. The number of bubbles decreases rapidly with decreasing ϕ until a value around $\phi = 0.001$. For lower values of ϕ, the number density of the bubbles saturates reaching the asymptotic limit where the initial small voids at the bottom of the bed merge quickly to form large slugs close to the inflow. Once the bed reaches the slugging regime, the number of bubbles in the bed does not change significantly since the large slugs dominate the fluidization region. In the cases considered, the superficial gas velocities were not high enough to lead to the transition to turbulent fluidization with lowering ϕ, thus bubble statistics for this regime were not acquired in this study.

The average bubble diameter versus ϕ for the two superficial gas velocities is shown in fig. 6. As expected, the average bubble diameter is inversely related to the bubble number density. For high ϕ, a considerable part of the momentum transferred by the fluidizing medium to the particles is dissipated at the wall in the tangential direction leading to slower motion of the particles and the formation of a large number of small bubbles. Low values of the specularity coefficient impose less hindrance on the motion of the particles in the near wall region,

resulting in higher solids velocities and subsequently to an increase of the average bubble diameter through the formation of the slugs. Concerning the bubble rise velocities, it was shown in [16] that the square root of the bubble diameter is proportional to the bubble rise velocity. Hence, according to bubble statistics extracted from the simulations, the mean rise velocity, in accordance with the bubble mean diameter, increases with decreasing specularity coefficient. This is shown in fig. 7(a) where the bubble rise velocity along the bed height is plotted for the high superficial gas velocity for four different specularity coefficients. A clear difference between the curves is the point of maximum velocity for varying ϕ. According to the bubble analysis already discussed, the small bubbles formed for high ϕ coalesce as they rise, and their velocity increases. The maximum bubble velocity for these cases occur at large bed heights, just before the splashing zone. With decreasing ϕ and the transition to the slugging behavior, the bubbles coalesce earlier and the maximum velocity moves towards smaller bed heights ($Y = 0.24$ for $\phi = 0.0005$). Fig. 7(b) shows the average bubble diameter versus the bed height for different values of ϕ. It is observed that for high ϕ, the variation of the bubble diameter along the bed height follows the bubble velocity and the bubbles continually grow until they reach the splashing zone. This trend is not followed anymore for low ϕ while the bed operates in the slugging regime. The diameter of the formed slugs continue to grow along the bed height even after the decrease in their rise velocity, indicating the increasingly significant bypassing effects at the upper part of the bed for low values of the specularity coefficient. Another interesting observation is that the average size of the new bubbles near the bottom of the bed (fig. 7(b)) is also dependent on ϕ. The average diameter of the new bubbles for $\phi = 0.5$ is approximately half the average diameter for the lowest ϕ for $Y < 0.05$ m. The momentum dissipation on the walls influences instantly the velocity of the solids, hindering their motion and resulting in the formation of smaller bubbles. As mentioned previously, for the statistical analysis of the bubbling behavior, the total sampling time was 27 sec at a frequency of 100Hz. The total number of bubbles tracked range from 15578 for $\phi = 0.0001$ to 81945 for $\phi = 0.5$. Of course this number does not refer to distinct bubbles since at such a sampling rate the evolution of a certain bubble is followed in successive frames. In order to assess an approximate number for the number of distinct bubbles considered in the statistical analysis we extract the average number of bubbles per frame and the average bubble velocity for each case. Then by assuming an average bed height of 40 cm, the number of distinct bubbles considered ranges roughly from 430 for $\phi = 0.0001$ to 800 for $\phi = 0.5$.

The momentum losses along the walls are clearly shown in fig. 8 where the pressure drop profiles are plotted for cases A and D for different values of ϕ. The pressure drop profiles vary almost linearly with bed height for $Y < 0.2$ m for all cases considered. For high superficial gas velocity case (case A), the pressure at the bottom for $\phi = 0.5$ is 18.5% higher than for $\phi = 0.0005$, while for case D this difference is 15.5%, indicating that the momentum losses depend on the superficial gas velocity, at least for the thin rectangular geometry considered in this study. The pressure difference at the bottom of the bed between the low specularity cases ($\phi = 0.0005$ and $\phi = 0.005$) is significantly lower for both cases considered due to the gas bypassing effects resulting in lower

momentum exchange between the gas and the solids and hence less momentum dissipation along the walls. Overall, the influence of the specularity coefficient on the bubble dynamics, especially for the thin rectangular beds investigated in this work, is decisive since it is shown that they are extremely sensitive to variations of this parameter. The physical interpretation of this sensitivity is the fact that low momentum dissipation along the walls (low ϕ), results in enhanced solids motion and the creation of larger and faster bubbles since more momentum is transferred from the gas to the solid phase.

Although the thin rectangular bed is a special case, since the wall surface to bed volume ratio is high, several important conclusions can be drawn. The bubble evolution is sensitive to the specularity coefficient since low values of ϕ result in the appearance of less bubbles with larger diameters and higher ascending velocities. For a certain value of the superficial gas velocity, very low values of ϕ ($\mathcal{O}(10^{-4})$) lead to transition of the fluidization behavior to the slugging regime, while for increasing ϕ the fluidization behavior tends towards the bubbling regime.

5.2. Influence of specularity coefficient on solids motion

The bubbling dynamics is closely related to the motion of the solids in the bed and after the detailed discussion of the effect of the specularity coefficient on the bubbling behavior we focus on the particle motion. As already discussed in the previous section, we employ the circulation flux as the main quantity of investigation since it is a continuous quantity across the bed containing information for both the solids vertical velocities and the cross-sectional areas of the upwards and the downwards motion of the particles. The bed averaged circulation flux, calculated as the spatial average in the vertical direction of the circulation rate profile for heights between 5 cm$< Y < 35$ cm, versus the specularity coefficient for two superficial gas velocities is presented in a semi-log plot in fig. 9. For each case, both the positive J_c^+ (upward) and the negative J_c^- (downward) fluxes are shown. Apart from the expected observation that the circulation fluxes increase at higher superficial gas velocity, they are smaller for large ϕ and they increase rapidly with decreasing values of specularity coefficients. This is also expected since the smaller the value of ϕ, the less momentum is transferred to the wall in the tangential direction and the faster the solids velocity. It is interesting to note the relation with the bubbling behavior. When the bed lies in the bubbling regime (i.e. $10^{-3} < \phi < 10^{-2}$) and the fluidizing region is dominated by a large number of small bubbles, the circulation flux is low, while it is much higher when the bed operates in the slugging regime (i.e. $\phi < 10^{-4}$). This is because of the higher velocity of the bubbles in the low ϕ case, as well as from the higher momentum transfer between the particles due to their collisions. For most of the values of ϕ tested, the upwards circulation flux is larger than the negative. This is attributed to the differences of the mean cross-sectional areas of upwards and downwards motion of the particles. The circulation fluxes J_c^+ and J_c^- at each bed height are calculated by spatial averaging over the parts of the cross-sectional area where the solids move accordingly. As a result, the circulation flux is inversely related to the respective

16

cross-sectional area and hence, for most specularity coefficients the average cross-sectional area covered with upwards moving particles is lower than the area of the downwards moving particles. A common feature in the two U_{in} cases is that for the lowest ϕ, $J_c^- > J_c^+$.

The profiles of the positive circulation fluxes which are averaged both temporally and spatially along the cross-sections of the bed show significant sensitivity on the specularity coefficient as presented in fig. 10 for the case with $U_{in} = 2.5U_{mf}$. The dependency is the same for the low superficial gas velocity case, and it is not presented here. The profiles of the large ϕ cases ($0.05 < \phi < 0.5$) do not show strong variation along the vertical direction of the bed. As the specularity coefficient decreases this trend changes. For intermediate values of ϕ, ($0.05 < \phi < 0.001$), the circulation flux increases from the bottom of the bed until $Y = 0.15$ m. For $0.15 < Y < 0.25$ m J_c^+ decreases and for the rest of the bed it increases again but more slowly. This variation of the positive circulation flux profiles is related to the bubbling behavior. In the high ϕ cases, the fluidization is dominated by a large number of small bubbles, and owing to the small static bed height, a considerable part of them reaches the splashing zone without merging with each other and hence the bubble diameters and rise velocities do not vary significantly along the bed. For decreasing specularity coefficients, the bubbling behavior changes and the small bubbles formed at the bottom of the bed, grow in size while moving upwards until $Y = 0.15$ m resulting in the increase of the circulation flux. Above this merging point, ($0.15 < Y < 0.25$ m), the bubbles coalesce forming significantly elongated bubbles that offer a passage for the excess gas of the bed due to the lower resistance of the flow, thus reducing the interaction with the solid phase and subsequently resulting in the gradual decrease of the circulation flux. For $Y > 0.25$ m, the large bubbles dominate the rest of the fluidized domain and rise with an increasing velocity causing the slow rise of J_c^+. The same mechanism results in the profile of J_c^+ for $\phi = 0.001$ with the difference that the maximum growth and merging points of the bubbles occur at lower positions along the bed. For $\phi = 0.0005$, the slugs are formed very close to the bottom and continually grow as they ascent leading to the increase of J_c^+ until the splashing zone. When the specularity coefficient used is even lower, the slugs are formed immediately and the circulation flux increases until $Y = 0.15$ m. Further upstream, they connect with previously created voids and the gas rises through them towards the splashing zone resulting in intensive gas-bypassing and as a result J_c^+ is decreases with increasing height in the bed.

The results for the total circulation time together with its components corresponding to the upwards and downwards solids motion are shown in a semi-log plot in fig. 11 for $U_{in} = 2.5U_{mf}$ and $U_{in} = 1.75U_{mf}$ versus ϕ. The circulation times, extracted according to the definition described in the previous section (eqs. 16, 17), are inversely related to the respective fluxes, hence they decrease with decreasing ϕ. Also, in accordance with the results presented in fig. 9, the circulation time depends on the superficial gas velocity and it decreases for faster fluidization.

5.3. 2D vs 3D

Although the thin rectangular bed is a frequently used experimental setup since it allows optical access and the bubbling dynamics can be directly measured, the effect of the wall boundary conditions along the front and back surfaces is important. A $2D$ computational domain imposes a periodicity of infinitely short length in the third dimension, thus neglecting the momentum dissipation occuring during the interaction of the solid phase with the front and back walls. In thin rectangular beds, owing to the large surface area of these walls, the absence of the wall-particle interaction is expected to have a significant influence the actual fluidization hydrodynamics. To elucidate the effect of dimensionality on the predicted hydrodynamic behavior we compare quantities characterizing the fluidization extracted from simulations conducted in $2D$ and $3D$ computational domains for different values of ϕ. Figure 12 (a) shows the voidage profile along the bed height for the cases with $U_{in} = 2.5 U_{mf}$ for $\phi = 0.0005$ and $\phi = 0.5$ simulated both in $2D$ and $3D$ domains, while fig. 12 (b) shows the pressure profile along the bed height for the same cases. In the absence of the momentum dissipation effects along the front and back walls, the voidage profiles and subsequently the predicted height of the splashing zone of the $2D$ cases are very close to each other. It is also observed that they agree quantitatively with the voidage profile of the low speculairty coefficient case simulated in $3D$, indicating that $2D$ simulaitons are not the expedient setup for describing the fluidization in thin rectangular beds. The pressure profiles of the $2D$ cases folllow the same trend. The pressure at the bottom of the bed predicted by the $2D$ setups is identical with the low ϕ three-dimensional simulation.

The analysis of the bubble evolution for the different cases considered is shown in fig. 13. Figure 13(a) shows the cumulative normalized frequency of the bubble diameters for the cases described above, while fig. 13(b) and (c) show the average bubble diameters and the average bubble velocities along the bed height respectively. It is observed that the bubble statistics for all the $2D$ cases are similar to the bubbling behavior predicted by the low ϕ three-dimensional computations. There is a discrepancy between the high ϕ three-dimensional simulation results and the rest of the cases considered which is consistent with the discussion presented in sec. 5.1, namely that the $2D$ results resembling the low specularity coefficient cases are dominated by larger bubbles which move faster towards the splashing zone. Finally, the circulation times were extracted for the $2D$ cases and their range was found to be $1.18 < t_c < 1.38$ s, for $0.0005 < \phi < 0.5$. The range of values of ϕ resulting in similar circulation times in the $3D$ simulations is $0.0001 < \phi < 0.0005$ with $1.16 < t_c < 1.63$ s.

5.4. Comparison with experiments

In the previous sections, it was shown that the influence of the specularity coefficient on the fluidization hydrodynamics and the solids motion is significant in thin rectangular beds. In the current section, the computational results are compared with the measurements of [24] in order to extract the correct values of ϕ that lead to the accurate description of the actual fluidization hydrodynamics. The computationally extracted circulation

times according to the definition followed in [24] (eqs. 18, 19) are compared with the experimentally measured times reported in [24] together with the value of ϕ which results in the correct value of t_c and the corresponding normalized sensitivity coefficient $S_{t_c,\phi} = d\left(ln(t_c)\right)/d\left(ln(\phi)\right)$ in table 5. The computationally extracted circulation times shown in table 5 are the closest to the experimentally measured values for the values of ϕ tested. The initial parametric sweep was performed with the values of ϕ reported in sec. 5.1 and resulted in a bounding interval where the upper and lower bounds of ϕ corresponded to lower and higher circulation times respectively compared to the experimentally measured values. In order to determine more precisely the appropriate values of the specularity coefficient for the different superficial gas velocities, more simulations were conducted with values of ϕ lying within the identified bounded interval until there was no significant difference between the experimentally measured and computationally predicted circulation times. Previous observations in the literature regarding the dependence of the correct value of ϕ on the superficial gas velocity are corroborated by the systematic parametric analysis presented in the current study. The value of ϕ resulting in agreement between the experimental and the computational circulation times for case with the highest U_{in} is $\phi = 0.05$. For the rest of the cases, it is observed that as the superficial gas velocity is reduced, the proper value of ϕ grows. For the case with the lowest U_{in} (case E), the proper value of the specularity coefficient is $\phi = 0.8$, an order of magnitude larger than for the case with the largest U_{in}. On the other hand, by comparing the circulation times between cases with the same U_{in} but different initial bed heights (h_{init}) we observe that there is no dependence on h_{init} and equal values of U_{in} result in equal values of ϕ. The normalized coefficients $S_{t_c,\phi}$ represent the sensitivity of the circulation times to changes of the specularity coefficient around the proper values of ϕ for each case. This definition of $S_{t_c,\phi}$ is non-dimensional and thus more useful for copmaring sensitivities of t_c to values of ϕ that differ by orders of magnitude.

Figure 14 shows four solids concentration maps (the time average probability of the presense of solids at a every point in the bed), each for a different value of the specularity coefficient together with the solids concentration map reconstructed from the image presented in [24]. The upper part of the plot refers to case A, while the lower part to case D. The plot presents a cross-validation of the proper values of ϕ extracted based on the fitting of the experimentally measured circulation times. The comparison is qualitative and shows that for the case with $U_{in} = 2.5U_{mf}$, the pattern predicted for both $\phi = 0.05$ and $\phi = 0.1$ agrees well with the experimentally extracted plot, confirming the validation procedure followed above. The same close agreement is observed for the lower superficial gas velocity case (case D), where the experimentally extracted plot is similar to the pattern predicted for $\phi = 0.5$, further supporting the extraction of ϕ by the fitting of the circulation times.

19

6. Conclusion

The Two-Fluid Model is used to simulate solid-gas fluidization in a thin rectangular bed, the so-called pseudo-$2D$ bed, in a realistic $3D$ setup taking into account the influence of the wall boundary conditions of the front and the back walls. This geometric setup has been extensively used in the literature since it is assumed that it resembles a simpler two-dimensional domain offering validation data for $2D$ simulations. It is shown that the wall effects are of paramount importance, rendering the fluidization hydrodynamics even more sensitive to the third dimension whose consideration is thus mandated.

A parametric analysis is conducted with repsect to the specularity coefficient in order to elucidate in a systematic way its influence on the fluidization hydrodynamics as reflected on the bubble statistics, the solids circulation fluxes and the circulation times. In the current study, the circulation fluxes and the circulation times are used to quantify the solids motion across the bed, while the bubble statistics summarize the gas phase hydrodynamics. It is shown that these quantities are highly sensitive to the value of the specularity coefficient, at least in the thin rectangular geometry considered, with low values of ϕ leading to high circulation fluxes and short circulation times driven by a fluidization behavior that is dominated by large slugs. For increasing values of ϕ, the fluidization behavior tends towards the bubbling regime and the increased momentum losses to the wall result in lower circulation fluxes and subsequently to larger circulation times.

The results presented in this work are compared with the experimental measurements of [24] in order to extract the values of ϕ that lead to the accurate description of the fluidization hydrodynamics. To achieve this a two-fold validation strategy is followed where we compare circulation times, derived from the circulation fluxes, as well as solid concentration maps, indicative of the time-averaged bubble presence across the bed. It is observed that the suitable value of ϕ for each case considered in this study depends on the superficial gas velocity, since with increasing superficial gas velocity, accurate prediction of the fluidization behavior is achieved with lower specularity coefficient. This indicates a possible dependence of the specularity coefficient on the slip velocity of the solid phase, as suggested in [14]. Further studies on the dependencies of the specularity coefficient are needed, as well as investigations on the sensitivity of the fluidization behavior on the boundary conditions in larger rectangular and cylindrical beds.

7. Acknowledgment

References

[1] M.A. van der Hoef, M. van Sint Annaland, N.G. Deen, and J.A.M. Kuipers. Numerical simulation of dense gas-solid fluidized beds: A multiscale modeling strategy. *Annual Review of Fluid Mechanics*, 40:47–70, 2008.

[2] B. G. M. van Wachem, J. C. Schouten, C. M. van den Bleek, R. Krishna, and J. L. Sinclair. Comparative analysis of cfd models of dense gassolid systems. *AIChE Journal*, 47(5):1035–1051, 2001.

[3] P. C. Johnson and R. Jackson. Frictional-collisional constitutive relations for granular materials, with application to plane shearing. *Journal of Fluid Mechanics*, 176:67–93, 3 1987.

[4] J.T. Jenkins. Boundary conditions for rapid granular flow: Flat, frictional walls. *Journal of Applied Mechanics*, 59:120–127, 1992.

[5] S. Schneiderbauer, D. Schellander, A. Lderer, and S. Pirker. Non-steady state boundary conditions for collisional granular flows at flat frictional moving walls. *International Journal of Multiphase Flow*, 43(0):149 – 156, 2012.

[6] M. Sommerfeld and N. Huber. Experimental analysis and modelling of particle-wall collisions. *International Journal of Multiphase Flow*, 25(67):1457 – 1489, 1999.

[7] F. Hernández-Jiménez, J. Sánchez-Prieto, A. Soria-Verdugo, and A. Acosta-Iborra. Experimental quantification of the particlewall frictional forces in pseudo-2d gas fluidised beds. *Chemical Engineering Science*, 102:257–267, 2013.

[8] S. Benyahia, M. Syamlal, and T.J. O'Brien. Evaluation of boundary conditions used to model dilute, turbulent gas/solids flows in a pipe. *Powder Technology*, 156(23):62 – 72, 2005.

[9] A. Almuttahar and F. Taghipour. Computational fluid dynamics of high density circulating fluidized bed riser: Study of modeling parameters. *Powder Technology*, 185(1):11 – 23, 2008.

[10] T. Li, Y. Zhang, J.R. Grace, and X. Bi. Numerical investigation of gas mixing in gas-solid fluidized beds. *AIChE Journal*, 56(9):2280–2296, 2010.

[11] T. Li, J. Grace, and X. Bi. Study of wall boundary condition in numerical simulations of bubbling fluidized beds. *Powder Technology*, 203(3):447 – 457, 2010.

[12] H. Zhong, J. Gao, C. Xu, and X. Lan. {CFD} modeling the hydrodynamics of binary particle mixtures in bubbling fluidized beds: Effect of wall boundary condition. *Powder Technology*, 230(0):232 – 240, 2012.

[13] X. Lan, C. Xu, J. Gao, and M. Al-Dahhan. Influence of solid-phase wall boundary condition on {CFD} simulation of spouted beds. *Chemical Engineering Science*, 69(1):419 – 430, 2012.

[14] T. Li and S. Benyahia. Revisiting johnson and jackson boundary conditions for granular flows. *AIChE Journal*, 58(7):2058–2068, 2012.

[15] T. Li and S. Benyahia. Evaluation of wall boundary condition parameters for gassolids fluidized bed simulations. *AIChE Journal*, 59(10):3624–3632, 2013.

[16] D. Geldart. *Gas Fluidization Technology*. John Wiley & Sons, 1986.

[17] M. Leva and M. Grummer. Correlation of solids turnover in fluidized bed. *Chemical Engineering Progress Symposium Series*, 48:307–312, 1952.

[18] E. Talmor and R.F. Benenati. Solids mixing and circulation in gas fluidized beds. *AIChE Journal*, 9(4):536–540, 1963.

[19] P.N. Rowe. Estimation of solids circulation rate in a bubbling fluidised bed. *Chemical Engineering Science*, 28(3):979–980, 1973.

[20] M Stein, Y.L Ding, J.P.K Seville, and D.J Parker. Solids motion in bubbling gas fluidised beds. *Chemical Engineering Science*, 55(22):5291 – 5300, 2000.

[21] Xianfeng Fan, David J. Parker, Zhufang Yang, Jonathan P.K. Seville, and Jan Baeyens. The effect of bed materials on the solid/bubble motion in a fluidised bed. *Chemical Engineering Science*, 63(4):943 – 950, 2008.

[22] A. Soria-Verdugo, L.M. Garcia-Gutierrez, S. Sanchez-Delgado, and U. Ruiz-Rivas. Circulation of an object immersed in a bubbling fluidized bed. *Chemical Engineering Science*, 66(1):78–87, 2011.

[23] K. Ohki and T. Shirai. Particle velocity in fluidized bed. In *Fluidization technology*, volume 2, pages 95–110. Hemisphere, 1976.

[24] S. Sánchez-Delgado, C. Marugán-Cruz, A. Soria-Verdugo, and D. Santana. Estimation and experimental validation of the circulation time in a 2d gassolid fluidized beds. *Powder Technology*, 235(0):669 – 676, 2013.

[25] D.G. Schaeffer. Instability in the evolution equations describing incompressible granular flow. *Journal of Differential Equations*, 66:19–50, 1987.

[26] C.K.K. Lun, S.B. Savage, D.J. Jeffrey, and N. Chepurniy. Kinetic theories for granular flow: inelastic particles in couette flow and slightly inelastic particles in a general flowfield. *Journal of Fluid Mechanics*, 140:223–256, 1984.

[27] D. Gidaspow. *Multiphase Flow and Fluidization: Continuum and Kinetic Theory Descriptions*. Academic Press, 1994.

[28] M. Syamlal, W. Rogers, and T.J. O'Brien. Mfix documentation theory guide. Technical report, U.S. Department of Energy, National Energy Technology Laboratory, 1993.

[29] S. Sánchez-Delgado, C. Marugán-Cruz, A. Acosta-Iborra, and D. Santana. Dense-phase velocity fluctuation in a 2-d fluidized bed. *Powder Technology*, 200:37–45, 2010.

[30] A. Bakshi, C. Altantzis, and A.F. Ghoniem. Towards accurate three-dimensional simulation of dense multi-phase flows using cylindrical coordinates. *Powder Technology*, (0):–, 2014.

[31] M. Syamlal. Mfix documentation numerical technique. Technical report, U.S. Department of Energy, National Energy Technology Laboratory, 1998.

[32] S.V. Patankar. *Numerical Heat Transfer and Fluid Flow*. Hemisphere Publishing Corporation, 1980.

[33] V.V.R. Natarajan and M.L. Hunt. Kinetic theory analysis of heat transfer in granular flows. *International Journal of Heat and Mass Transfer*, 41(13):1929 – 1944, 1998.

[34] Antonio Busciglio, Giuseppa Vella, Giorgio Micale, and Lucio Rizzuti. Analysis of the bubbling behaviour of 2d gas solid fluidized beds: Part i. digital image analysis technique. *Chemical Engineering Journal*, 140(13):398 – 413, 2008.

Table 1: Details from numerical studies investigating the influence of specularity coefficient on fluidization

Study	Geometry	System	Dimensions (width x height x depth)	ϕ
Benyahia et al. 2005 [8]	2D	Dilute Riser	N/A	0, 0.02, 1
Almuttahar et al. 2008 [9]	2D	CFB Riser	0.076 x 6.1 m	0, 0.1, 0.5, 1
Li et al. 2010 [10]	2D-3D	BFB	0.076 x 1.83 m	0, 0.005, 0.05, 0.5, 1
Li et al. 2010 [11]	3D	BFB	0.3 x 0.7 x 0.015 m	0.001, 0.005, 0.05, 0.5
Zhong et al. 2012 [12]	2D	BFB	0.184 x 0.4 m	0, 0.0005, 0.005, 0.05, 0.5, 1
Lan et al. 2012 [13]	2D	SFB	0.15 x 1.4 m	0, 0.01, 0.05, 0.2, 1

Table 2: Circulation flux correlations

Study	Solids Circulation Flux $[kg/m^2s]$	Method
Talmor and Benenati, 1963 [18]	$J = 758\,(U_{in} - U_{mf})\,exp(-6.63d_m)$	Experimental
Rowe, 1973 [19]	$J = 0.6\rho_m(1 - \varepsilon_{mf})\,(U_{in} - U_{mf})$	Two phase theory
Geldart, 1986 [16]	$J = Y(\beta_w + 0.38\beta_d)\rho_m(1 - \varepsilon_{g,mf})\,(U_{in} - U_{mf})$	Two phase theory

Table 3: Cases tested

Case	h_{init} [cm]	U_{in}/U_{mf}
A	30	2.5
B	30	2.25
C	30	2.0
D	30	1.75
E	30	1.5
K	50	2.5
N	50	1.75

Table 4: Simulation parameters

Quantity	Value
Bed height, m	1.5
Bed width, m	0.5
Bed thickness, m	0.005
Gas density, kg/m^3	1.225
Gas viscosity, kg/ms	$1.8\text{x}10^{-5}$
Solid material	Glass spheres
Particle diameter, μm	677.8
Particle density, kg/m^3	2500
Particle-particle restitution coefficient	0.9
Particle-wall restitution coefficient	0.8
Specularity coefficient	$0.0001, 0.0005, 0.001, 0.005, 0.01, 0.05, 0.1, 0.5$
Angle of internal friction, ^{o}	30
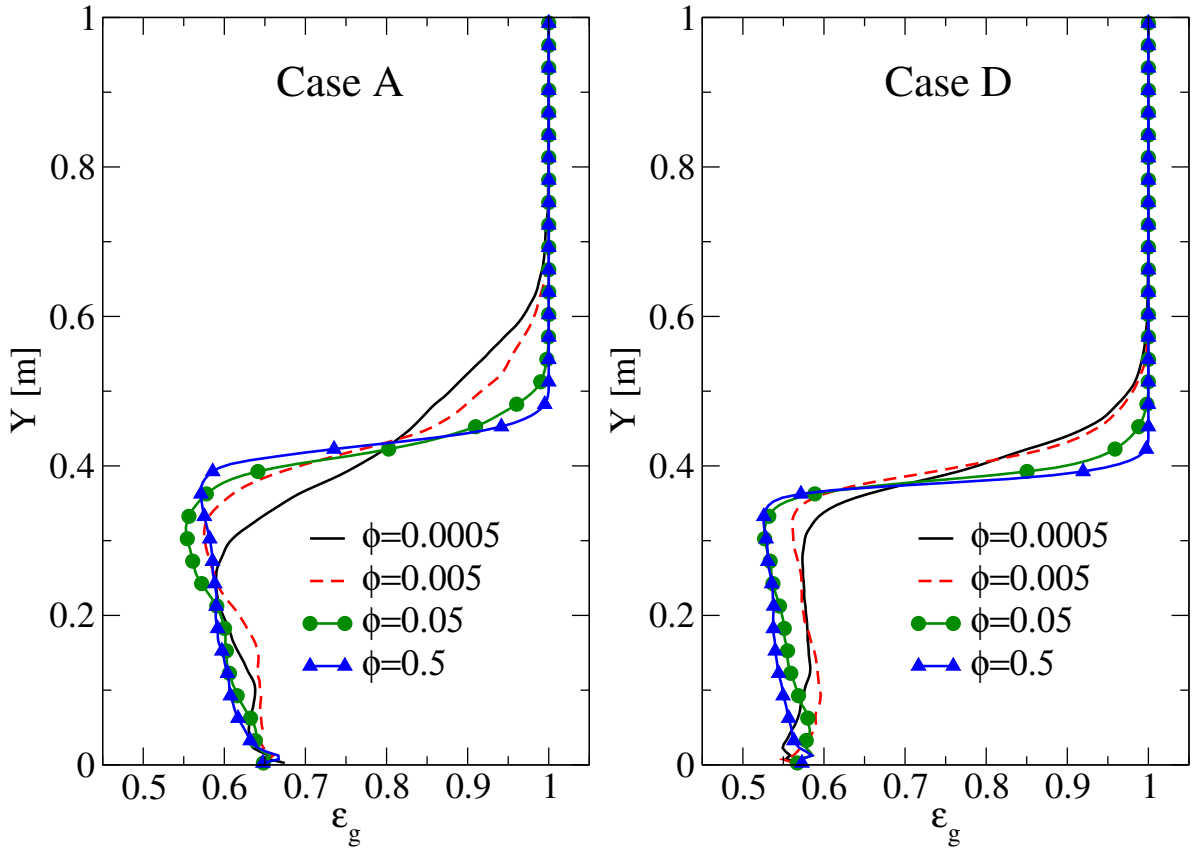
Figure 1: Solids holdup profiles for different values of the specularity coefficient with $U_{in} = 2.5U_{mf}$ (Case A) and $U_{in} = 1.75U_{mf}$ (Case D).
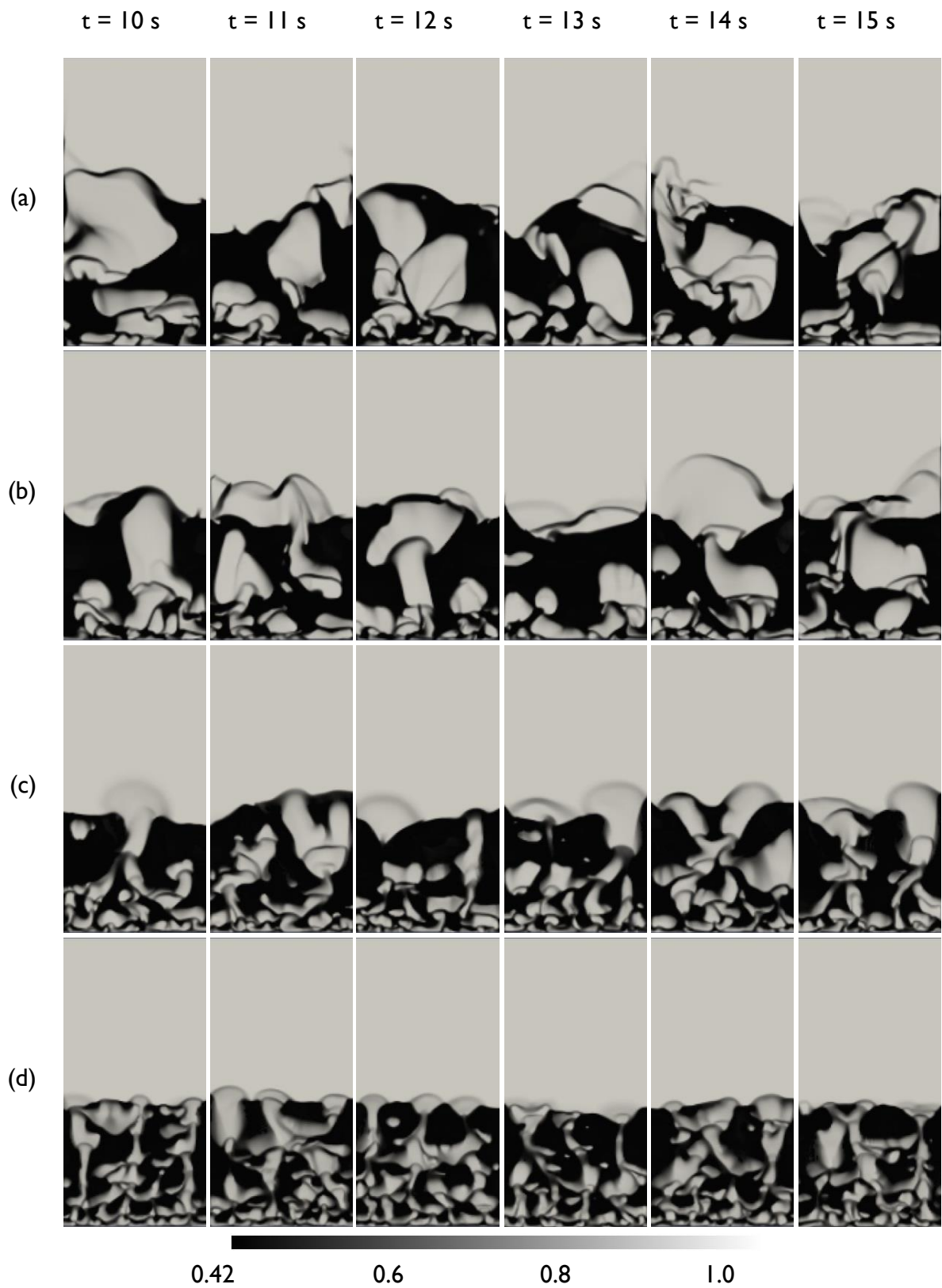
Figure 2: Instantaneous voidage contours in greyscale at six different times for $U_{in} = 2.5U_{mf}$ (Case A) for a) $\phi = 0.0005$, b) $\phi = 0.005$, c) $\phi = 0.05$ and d) $\phi = 0.5$
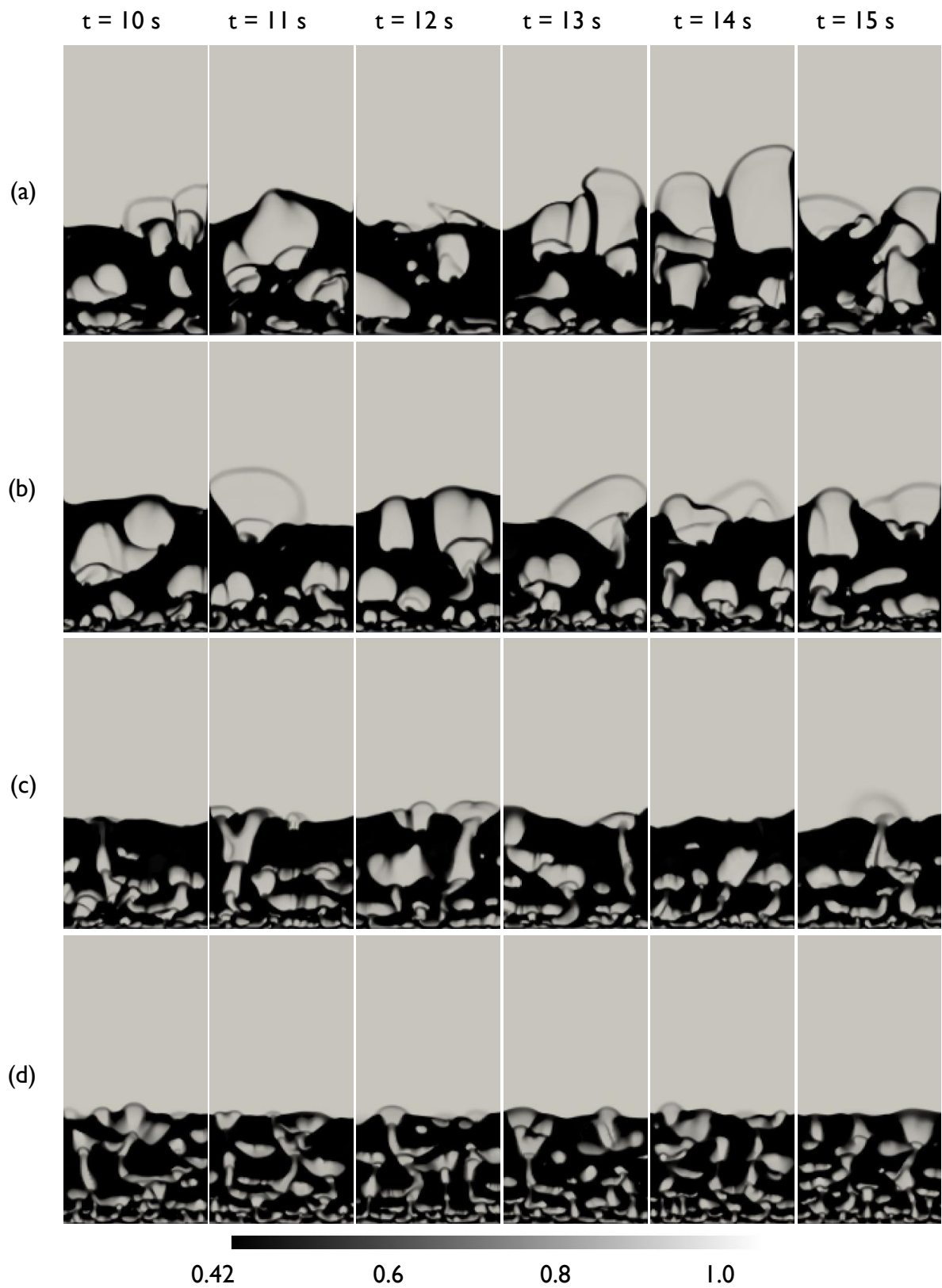
Figure 3: Instantaneous voidage contours in greyscale at six different times for $U_{in} = 1.75 U_{mf}$ (Case D) for a) $\phi = 0.0005$, b) $\phi = 0.005$, c) $\phi = 0.05$ and d) $\phi = 0.5$
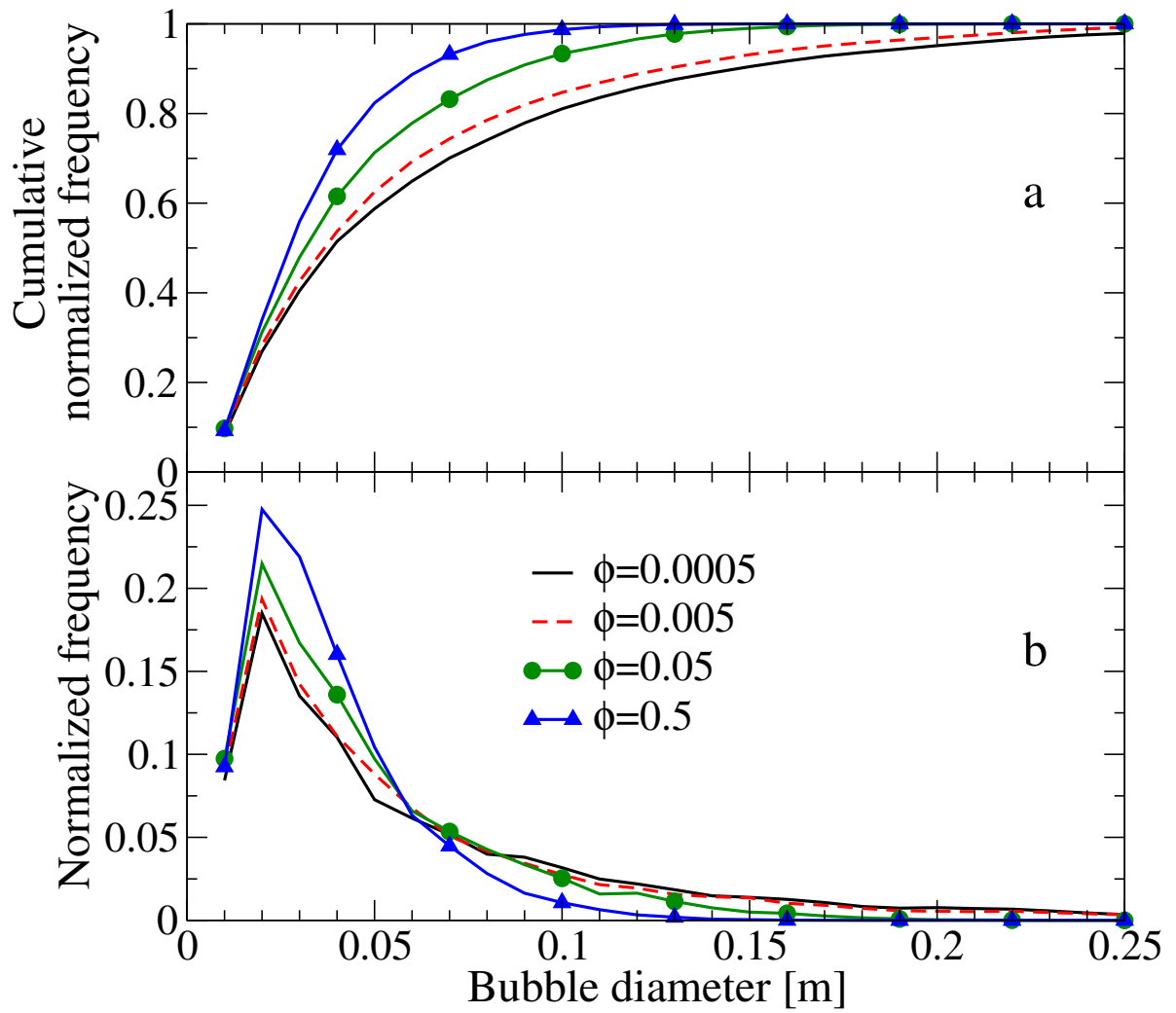
Figure 4: Cumulative normalized frequency of the bubble diameter (a) and normalized frequency of the bubble diameter (b) with repsect to different values of the specularity coefficient for $U_{in} = 2.5U_{mf}$ (Case A)
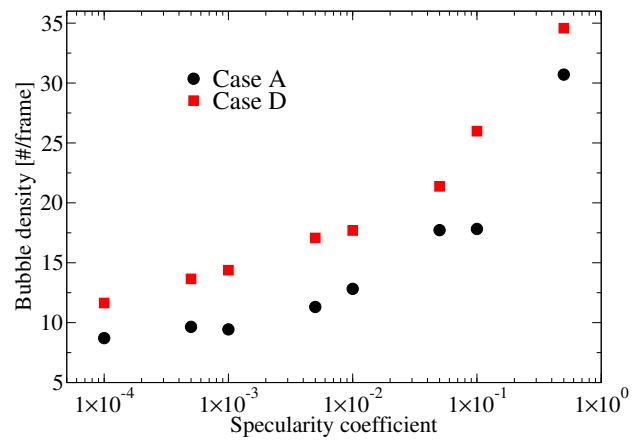
Figure 5: Bubble number density expressed as the average number of bubbles per frame versus the specularity coefficient for two different superficial gas velocities (Cases A and D)
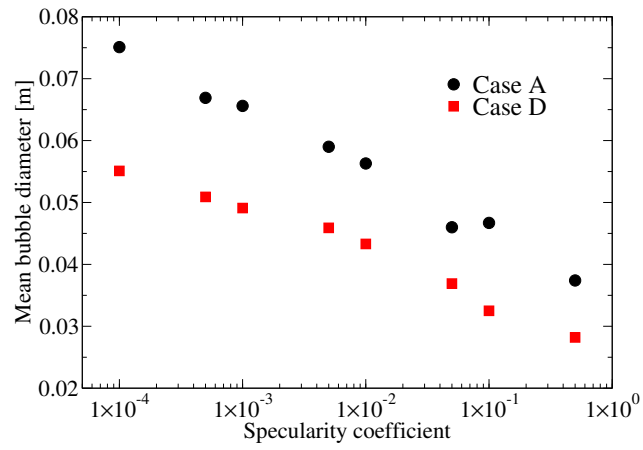
Figure 6: Mean bubble diameter versus the specularity coefficient for two different superficial gas velocities (Cases A and D)
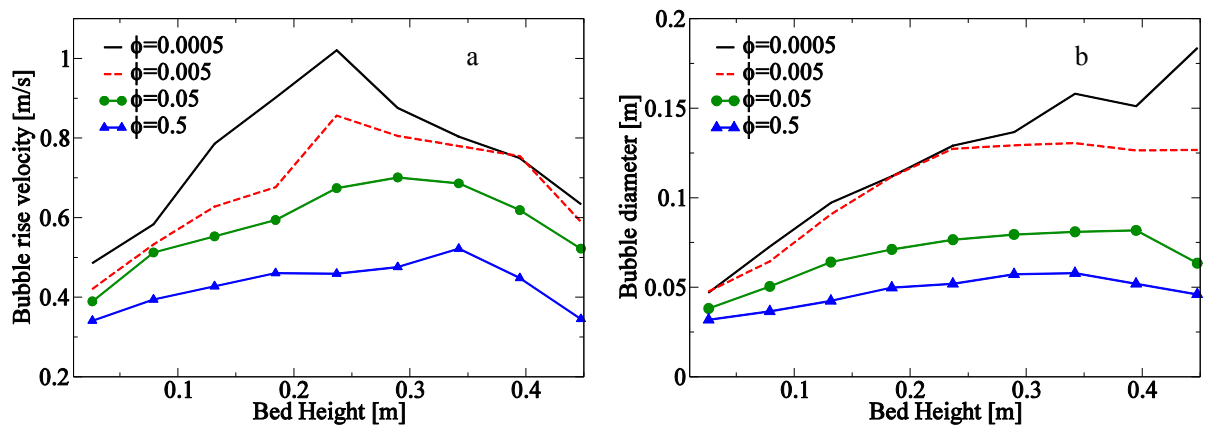
Figure 7: Average bubble rise velocities (a) and average bubble diameters (b) along the bed height for different values of the specularity coefficient for the case with $U_{in} = 2.5U_{mf}$ (Case A)
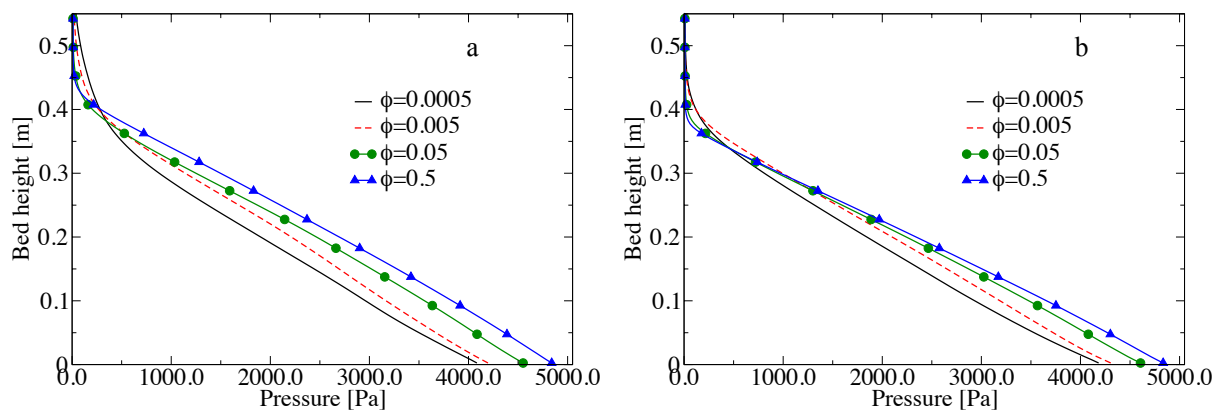
Figure 8: Pressure profile for the case with $U_{in} = 2.5 U_{mf}$ (Case A) (a) and for the case with $U_{in} = 1.75 U_{mf}$ (Case D) (b) along the bed height for different values of the specularity coefficient
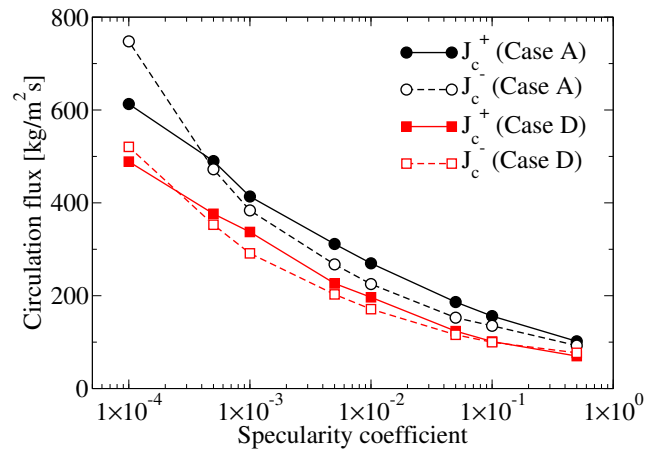
Figure 9: Spatially and temporally averaged positive (upwards) and negative (downwards) circulation fluxes versus specularity coefficient for two different superficial gas velocities (Cases A and D)
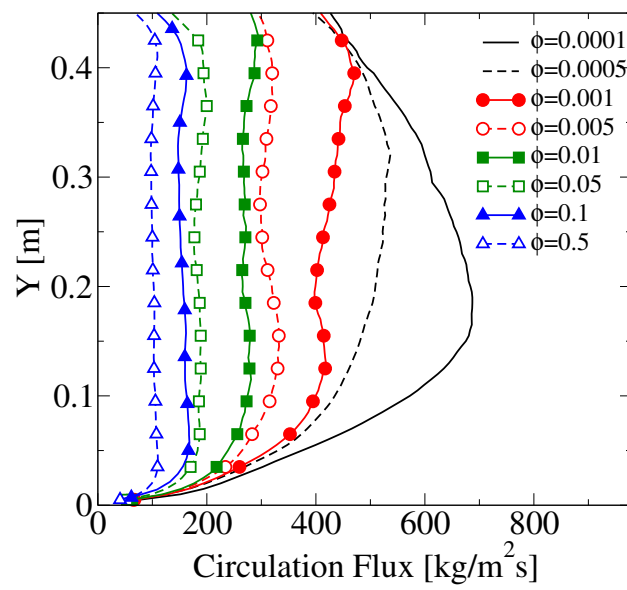
Figure 10: Positive circulation flux profiles along the bed height for different values of the specularity coefficient for $U_{in} = 2.5U_{mf}$ (Case A)
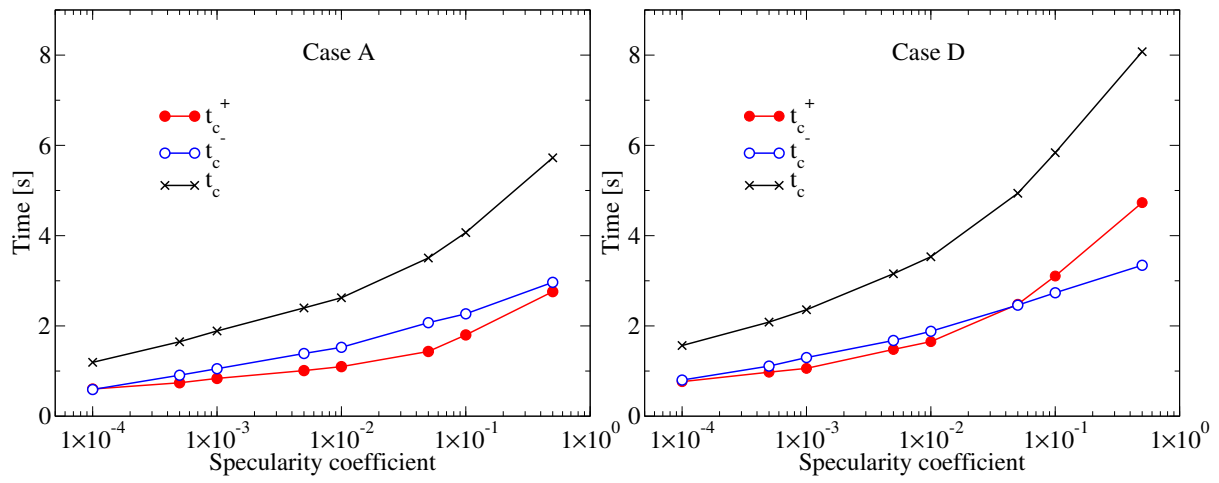
Figure 11: Upwards, downwads and total circulation times vs specularity coefficient or two different superficial gas velocities (Cases A and D)
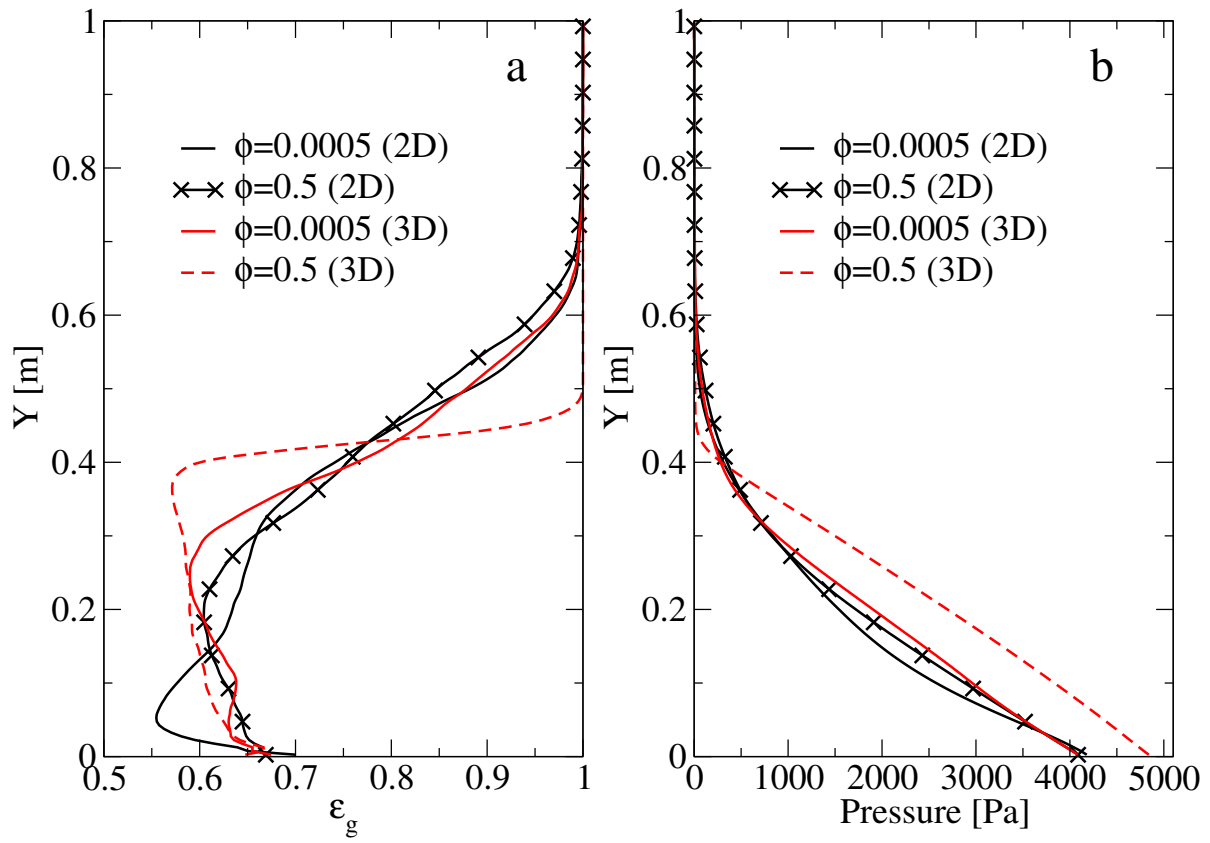
Figure 12: Voidage profiles (a) and pressure profiles (b) for different values of the specularity coefficient with $U_{in} = 2.5U_{mf}$ in 2D and 3D geometries
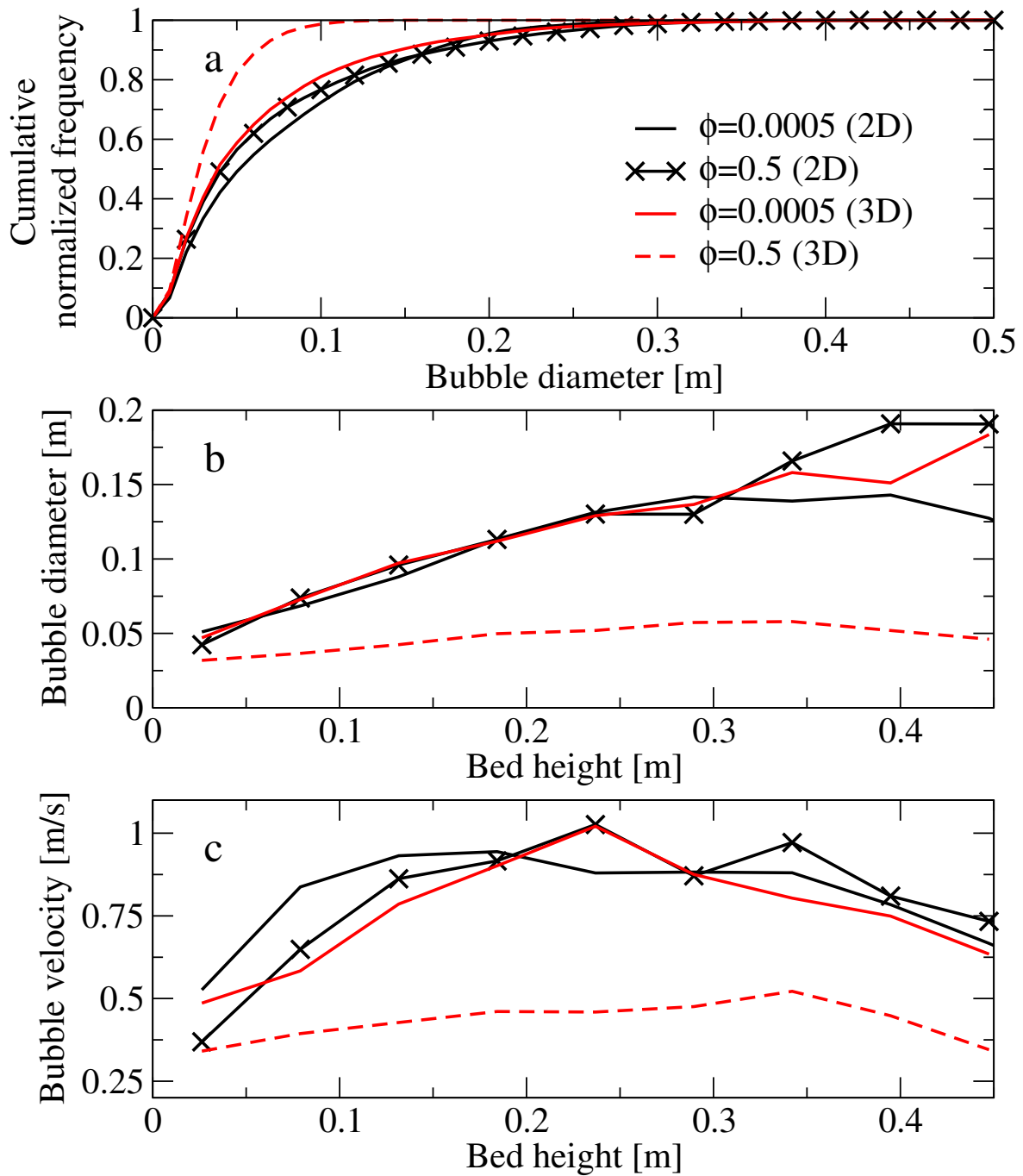
Figure 13: Cumulative normalized frequency of the bubble diameters (a) average bubble diameters along bed height (b) and average bubble velocities along the bed height (c) for different values of the specularity coefficient with $U_{in} = 2.5U_{mf}$ in 2D and 3D geometries

Table 5: Experimentally measured and computationally extracted circulation times for different superficial gas velocities with the corresponding specularity coefficient

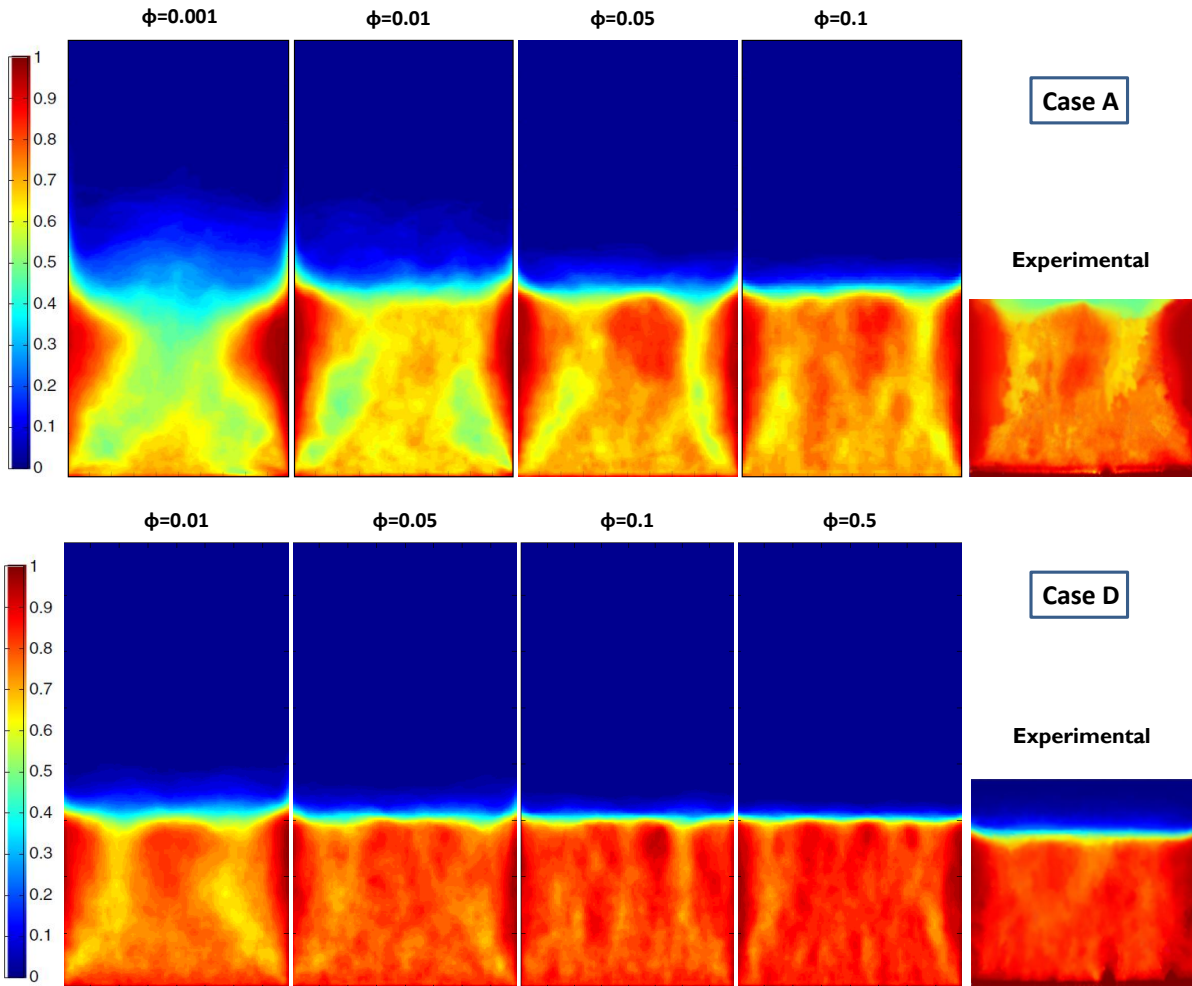| Case	U_{in}/U_{mf}	$t_c[s]$ (Experimental)	$t_c[s]$ (Computational)	ϕ	$S_{t_c,\phi}$
A	2.5	8.28	8.19	0.05	0.136
B	2.25	11.56	11.39	0.14	0.150
C	2.0	12.16	12.66	0.2	0.188
D	1.75	15.13	16.2	0.5	0.122
E	1.5	23.77	23.32	0.8	0.252
K	2.5	14.25	13.75	0.05	0.184
N	1.75	26.17	26.11	0.5	0.131

Figure 14: Computationally extracted solids concentration maps for different values of the specularity coefficient together with the experimentally measured map for two different superficial gas velocities (Cases A and D)